Uncertainty in Inverted Pendulum Thrust Measurements

J. Mackey,[1] T. Haag[2], H. Kamhawi[3]
NASA Glenn Research Center, Cleveland, Ohio 44135

S. Hall[4], and P. Peterson[5]
Vantage Partners LLC, Brook Park, Ohio 44142

An uncertainty analysis of a common configuration of electric propulsion thrust stand is presented. The analysis applies to inverted pendulum thrust stands operating in a null-coil configuration with in-situ calibration. Several sources of bias and precision uncertainty are discussed, propagated, and combined to form conservative estimates of the relative and absolute thrust uncertainties. A case study of the NASA Glenn Research Center Vacuum Facility 6 thrust stand is presented. For the thruster investigated, the uncertainty was estimated to be ±6.9mN over the entire span of thrust. This uncertainty represents a maximum instrument bias introduced by the thrust stand. The paper does not address repeatability of actual thrust measurements, as this is generally beyond the influence of the thrust stand and can be dependent on a large number of factors.

I. Nomenclature

α	=	Shunt thermal sensitivity
A_i	=	Transient regression coefficients
a,b	=	Calibration regression coefficients
c	=	Stand damping coefficient
C_i	=	Calibration force
e_i	=	Relative uncertainty
g	=	Acceleration due to gravity
k	=	Stand stiffness
m	=	Total stand mass including thruster and thrust stand components
m_i	=	Calibration mass
M	=	Calibration pulley moment
n	=	Calibration sample size
N	=	Null coil force
S_b	=	Calibration standard deviation
r	=	Calibration pulley radius
T	=	Thrust
t	=	Temperature
U	=	Absolute uncertainty
V	=	Null coil voltage
$x, \dot{x}$	=	Stand displacement, stand velocity
γ	=	Stand inclination angle
θ	=	Thrust vector angle
φ	=	Calibration alignment angle
ω	=	Stand natural frequency

[1] Jonathan.a.mackey@nasa.gov, Engineer, Electric Propulsion Systems, AIAA Member.
[2] Thomas.w.haag@nasa.gov, Engineer, Electric Propulsion Systems, AIAA Member.
[3] Hani.kamhawi-1@nasa.gov, Engineer, Electric Propulsion Systems, AIAA Associate Fellow.
[4] Scott.j.hall@nasa.gov, Engineer, Electric Propulsion Systems, AIAA Member.
[5] Peter.y.peterson@nasa.gov, Engineer, Electric Propulsion Systems, AIAA Associate Fellow.

II. Introduction

NASA continues to evolve a human exploration approach for beyond low-Earth orbit and to do so, where practical, in a manner involving international, academic, and industry partners [1]. Towards that end, NASA publicly presented a reference exploration concept at the Human Exploration and Operations Mission Directorate (HEOMD) Committee of the NASA Advisory Council meeting on March 28, 2017 [2]. This approach is based on an evolutionary human exploration architecture, expanding into the solar system with cislunar flight testing and validation of exploration capabilities before crewed missions beyond the Earth-Moon system and eventual crewed Mars missions.

High-power solar electric propulsion is one of those key technologies that has been prioritized because of its significant exploration benefits. Specifically, for missions beyond low Earth orbit, spacecraft size and mass can be dominated by onboard chemical propulsion systems and propellants that may constitute more than 50 percent of spacecraft mass. This impact can be substantially reduced through the utilization of Solar Electric Propulsion (SEP) due to its substantially higher specific impulse. Studies performed for NASA's HEOMD and Science Mission Directorate have demonstrated that a 40-kW-class SEP capability can be enabling for both near term and future architectures and science missions [3]. In addition, a high-power, 40 kW-class Hall thruster propulsion system provides significant capability and represents, along with flexible blanket solar array technology, a readily scalable technology with a clear path to much higher power systems.

Accordingly, since 2012, NASA has been developing a 14-kW-class[6] Hall thruster electric propulsion string that can serve as the building block for realizing a 40-kW-class SEP capability, in addition to the decades of electric propulsion development and flight programs conducted at NASA Glenn Research Center (GRC) [4]. The 14-kW Hall thruster electric propulsion string development, led by the NASA GRC and the Jet Propulsion Laboratory (JPL), began with maturation of the high-power Hall thruster and Power Processing Unit (PPU). The technology development work has transitioned to Aerojet Rocketdyne via a competitive procurement selection for the Advanced Electric Propulsion System (AEPS) contract. The AEPS contract includes the development, qualification, and delivery of multiple flight 14-kW-class electric propulsion strings. The AEPS Electric Propulsion (EP) string consists of the Hall thruster, power processing unit (including digital control and interface functionality), xenon flow controller, and associated intra-string harnesses. NASA continues to support the AEPS development leveraging in-house expertise, plasma modeling capability, and world-class test facilities. NASA also executes AEPS and mission risk reduction activities to support the AEPS development and mission application.

As part of HERMeS and AEPS efforts, NASA has completed multiple performance characterization test campaigns to access the capabilities of the HERMeS thruster [5-10]. Although there are a large number of parameters of interest when characterizing a propulsion system, including plasma plume characterization, thermal performance, spacecraft charging and interaction, erosion and lifetime, and electromagnetic radiation, arguably the primary concern of any thruster development activity is the thruster performance. This is typically characterized by metrics such as efficiency and specific impulse, calculations of which are reliant on some characterization of the thrust produced by the device, making accurate and reliable thrust measurement a critical interest for electric propulsion systems [13-17]. Whenever possible, and by industry standard, for EP devices this is done by direct thrust measurement [13]. This measurement is often challenging due to the low thrust to weight ratio typical to EP thrusters and requires extremely precise measurement techniques and apparatus. Often, thrust stands of either the inverted pendulum or torsional balance type are used. NASA GRC has led the electric propulsion community in the development and implementation of electric propulsion thruster measurements over the past several decades [11-13]

In this work uncertainty in thrust measurements has been quantified with a heuristic approach to capture instrument resolution, measurement bias, calibration precision, and uncertainty propagation influences common in thrust measurement. An example analysis has been performed for NASA GRC Vacuum Facility 5 (VF-5) and Vacuum Facility 6 (VF-6) null-type inverted pendulum thrust stands. The VF-5 and VF-6 analysis is specific with the HERMeS Technology Demonstration Units (TDU) thruster, however information presented in this work is extensible to any electric propulsion power level that employs a NASA GRC inverted pendulum null-type thrust stand that has been tuned to the propulsion system mass and thrust level. The NASA GRC high-power thrust stands in VF-5 and VF-6 are shown in Figure 1 with the NASA HERMeS TDU-3 Hall thruster. The thrust uncertainty has been calculated for a range of thrust levels typical for HERMeS TDU thrusters and has been found to be ±6.9mN over a wide throttling range. The estimation of thrust uncertainty is critical to project and mission planning and is required to advance the technology of electric propulsion systems. In addition to estimating the nominal uncertainty

[6] Complete electric propulsion system power.

level, the contribution and comparison of different uncertainty sources has been investigated. The contribution of uncertainty sources is of critical interest to both designing new thrust stands and improving existing ones. A discussion on the NASA GRC VF-6 thrust stand, Figure 1(b) will outline some of the improvements introduced as a result of this uncertainty work. The analysis is intended to be detailed but an exhaustive list of uncertainty sources is not practical, therefore additional terms which have not been quantified are discussed to plan for future improvements to the model.

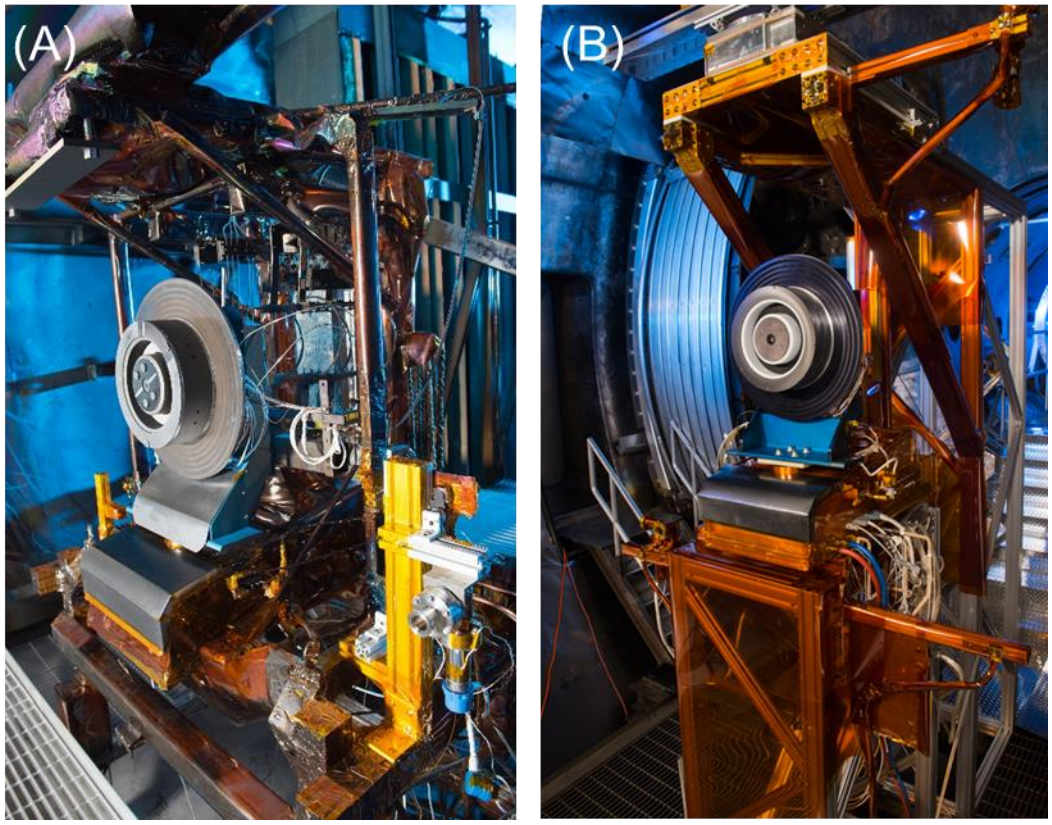

Figure 1. NASA GRC High-Power Thrust Stands in VF-5 (A) and VF-6 (B) with the HERMeS TDU-3 Hall thruster.

III. Model of an Inverted Pendulum Thrust Stand

A sketch of the simplified model of the thrust stand under consideration is presented in Figure 2. The inverted pendulum stand was modeled as a nominal one degree of freedom four-bar linkage with inherent stiffness and viscous damping elements. The weight of the thruster was assumed constant, such that propellant mass loss was zero or insignificant. The thruster was assumed to behave as a fixed mass, which moved with the thrust stand and produced a steady thrust force. The thrust stand rigidly supported the thruster in every direction other than the sensitive thrust direction. The thrust stand was investigated under two operating modes: calibration (Figure 2a and 2b), and thruster operation (Figure 2c). The in-situ calibration mechanism (Figure 2b) provides a means of establishing a relation between the load on the stand and the current in a counteracting voice coil called the null coil, this is termed the "null-coil mode". The stand may also be operated in a "displacement mode" configuration, in which the stand is free to displace in one direction and load is calibrated against stand position. The analysis of this work focuses on the null-coil mode of operation, but many of the same terms and methods could apply to both. Though, in many cases the null-coil mode of operation may lead to more reliable measurements, this work does not attempt to make recommendations on thrust stand operating principals. The reader is directed to Reference [13] for more information on best practices in thrust measurement and thrust stand operating principles. The general method outlined in this work can be extended to a number of thrust stands and thrusters. Sources of uncertainty outlined in Figure 2 will be explained in greater detail in the Uncertainty Quantification section to follow. Subscripts 'i' in

Figures 2a and 2b indicate terms which are sensitive to individual calibration masses. In general, a number of calibration masses are employed to ensure a reliable calibration scheme across the range of thrust levels of interest. The subscript 'T' in Figure 2c indicates terms which are sensitive to the thrust measurement.

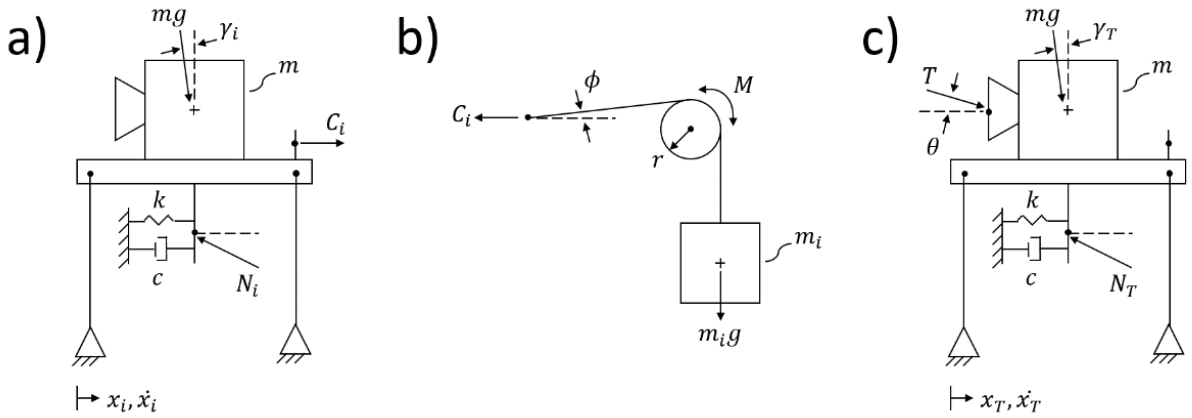

Figure 2. Simplified model of a thrust stand operating under calibration mode (a and b) and thruster operating mode (c). Subscripts 'i' indicate terms sensitive to individual calibration masses. Subscripts 'T' indicate terms sensitive at the time of thrust measurement.

In an ideal null-coil inverted pendulum thrust stand the stand position x is fixed, stand inclination γ is fixed, and stand velocity $\dot{x}$ is zero. Furthermore, the calibration loads C_i are perfectly known, the null-coil shunt voltages V_i are perfectly known, and the thrust vector is oriented directly along the thrust stand line of motion. In practice these simplifications may lead to erroneous measurements. It is the objective of this work to attempt to quantify these non-zero terms. It is not the objective of this work to investigate thruster operating behavior or thrust stand repeatability. This uncertainty quantification is an estimate of the "design-stage" or "single-measurement" type uncertainty analysis, and represents a conservative estimate of the farthest that a thrust value is likely to be from actual. In general both bias and precision errors are accounted for and propagated with a confidence interval of 95%. The absolute thrust stand resolution and repeatability may be addressed in a future work.

IV. Uncertainty Quantification

A. Uncertainty Propagation

Uncertainty of a dependent variable was approximated using the method outlined by Figliola and Beasley [18] by means of a truncated Taylor series expansion of the measurement formula. Similarly, the uncertainty analysis is as much as possible in accordance with the work of Abernethy et. al [19], Moffat [20], and a more recent NASA Measurement Uncertainty Analysis Principles and Methods Handbook [21]. Absolute uncertainties U_x of the independent measurands were accounted for from each independent source of uncertainty whenever possible. The truncated Taylor series approximation of uncertainty propagation of an arbitrary function $y = f(x)$ can be expressed as,

$$\bar{y} \pm U_y = f(\bar{x} \pm U_x) \approx f(\bar{x}) \pm \left.\frac{df}{dx}\right|_{x=\bar{x}} U_x.$$

Absolute uncertainties were normalized to relative uncertainties for the dependent variable e_{y_i}, normalized with nominal values of the dependent variable to allow combination of different sources. The relative sources were combined using a root sum of square (RSS) type inner-product. The RSS combined relative uncertainty sources lead to an estimated total relative uncertainty. The RSS method provides a suitable combination strategy for statistically independent sources of uncertainty (zero covariance for any two error sources). A more conservative estimate of uncertainty may be to simply arithmetically add the different sources of uncertainty to obtain a total uncertainty, but this generally leads to over estimation of uncertainty [19,21]. The definition of relative uncertainty for some uncertainty source x, and the RSS combination of a number of sources is expressed as,

$$e_{y_x} = \frac{1}{\bar{y}} \frac{\partial y}{\partial x}\Big|_{x=\bar{x}} U_x,$$
$$e_{Total} = \sqrt{e_{y_1}^2 + e_{y_2}^2 + e_{y_3}^2 + \cdots}.$$

In many cases analytic formulation of all sources of uncertainty may become tedious, in which case a method like Monte-Carlo simulation may be employed. For the analysis of this work the sources investigated could be handled analytically, resulting in meaningful closed form terms to be used for stand design and improvement.

B. Uncertainty Sources

A number of factors contribute to the uncertainty of inverted pendulum thrust measurements. The main sources of measurement uncertainty are the calibration procedure, drift of the stand between calibrations, unknown thrust vector relative to the stand, and the data acquisition uncertainty. Figures 2a and 2b depict many of the factors to consider during calibration of the stand. When operating in null mode the measured thrust is proportional to the null coil current, often measured as a voltage drop across a fixed shunt resistor. The relation between null coil shunt voltage and thrust was periodically evaluated by means of a calibration procedure. An example calibration regression formula is a simple linear regression which has been used for this work. The thrust T is dependent on the null coil shunt voltage V_T, two calibration factors a and b, and a total thrust uncertainty U_T as follows,

$$T = a + b\,V_T \pm U_T.$$

The objective of the current section is to identify sources of uncertainty which may contribute to the total thrust uncertainty U_T. Table 1 outlines nine sources of uncertainty including factors relating to calibration, thrust vector, and stand drift. In many cases so called "best-practices" of a thrust stand operation are intended to minimize influence of each of the terms listed. The intention of this work is to establish a quantitative estimate of each term, rather than to neglect or ignore a term due to its small nature. Extending this analysis to other thrust stands and other thrusters may introduce additional sources or may remove some sources listed. Inclusion of any source is at the discretion of the researcher. In general, removing or neglecting a source does not significantly alter the final total uncertainty as a result of the RSS combination method employed, unless the source is a major contributor. Including additional small terms generally leads to a somewhat conservative estimate of uncertainty.

Table 1: Sources of uncertainty- overbar represents nominal value, tilde represents average value.

Source	Relative Uncertainty	Parameters of Interest	Parameter Description
Thrust vector	$e_\theta = 1 - \cos(\theta)$	θ	Thrust vector angle
Stand displacement drift	$e_x = \frac{k\lvert x_T - \widetilde{x_t}\rvert}{\bar{T}}$	$\lvert x_T - \widetilde{x_t}\rvert$, $k = \omega_n^2 m$	Stand position drift, Stiffness
Stand velocity drift	$e_{\dot{x}} = \frac{c\lvert \dot{x}_T - \widetilde{\dot{x}_t}\rvert}{\bar{T}}$	$\lvert \dot{x}_T - \widetilde{\dot{x}_t}\rvert$, c	Stand velocity drift, Damping coefficient
Stand inclination drift	$e_\gamma = \frac{mg\ \sin\lvert \gamma_T - \widetilde{\gamma_t}\rvert}{\bar{T}}$	$\lvert \gamma_T - \widetilde{\gamma_t}\rvert$, mg	Stand inclination drift, Thruster weight
Shunt thermal drift	$e_{shunt} = \frac{\alpha\lvert t_T - \widetilde{t_t}\rvert}{\bar{R}_{shunt}}$	$\lvert t_T - \widetilde{t_t}\rvert$, α, $\bar{R}_{shunt}$	Temperature drift, Thermal sensitivity, Nominal resistance
Calibration slope repeatability	$e_{slope} = \frac{S_b\overline{V_T}}{\bar{T}} = S_b\left(\frac{1}{b} - \frac{a}{b\bar{T}}\right)$	S_b	Calibration gain standard deviation
Calibration regression correlation	$e_{S_{xy}} = \frac{\sqrt{\frac{\sum(C_i - [a + bV_i])^2}{n-2}}}{\bar{T}}$	C_i, $a + bV_i$	Calibration force, Calibration regression
DAQ uncertainty	$e_{V_i} = \frac{U_{V_i}}{\overline{V_T}} = U_{V_i}\frac{\bar{T} - a}{b}$	U_{V_i}	Data acquisition uncertainty
Calibration uncertainty	$e_{C_i} = \frac{1}{\bar{T}}\frac{\partial T}{\partial C_i}U_{C_i}$	U_{C_i}	Calibration uncertainty, see table 2

The first term in Table 1 represents the possibility for a discrepancy between the thrust vector orientation and the thrust stand's line of motion. A conservative estimate for the maximum possible angle between the thruster's thrust vector orientation and the direction of motion of the stand should be used. This angle may account for mounting tolerance, mounting variability, asymmetry in the thruster, or asymmetry in the vacuum facility. In general, effort must be made to reduce this angle as much as possible, but a conservative estimate is still helpful for the purposes of estimating the total possible uncertainty.

The second through fifth terms account for a drift type uncertainty source. In an ideal situation the state of the stand is identical during calibration and all thrust measurements. In practice the state of the thrust stand can vary between calibration and thrust measurement, this difference of state is termed drift. A number of factors may cause thrust stand drift including thermal expansion, vacuum facility distortion, external mechanical vibrations, and other external interference. Three main sources of drift uncertainty are outlined in Table 1 including stand displacement drift, stand velocity drift, and stand inclination drift. In all cases the uncertainty source is dependent on a term composed of a difference between calibration and thrust measurement of a thrust stand state parameter. For stand displacement drift the difference $\lvert x_T - \widetilde{x_t}\rvert$ is of interest, for stand velocity drift the difference is $\lvert \dot{x}_T - \widetilde{\dot{x}_t}\rvert$, and for stand inclination drift the difference is $\lvert \gamma_T - \widetilde{\gamma_t}\rvert$. At a minimum the state difference between calibration and thrust measurement is the resolution of the control system used to manage the drift. In practice the difference may be larger than the resolution of the control system, and may depend on a large number of factors such as control system tuning. For instance, steady-state error of a poorly tuned control loop can lead to differences significantly larger than the control system resolution. The three drift uncertainty terms introduce a stiffness to thrust ratio $k/\bar{T}$, damping to thrust ratio $c/\bar{T}$, and the weight to thrust ratio $mg/\bar{T}$. These three terms can be calculated for different thrust stands and thrusters, and are critical to determining generally the largest sources of uncertainty in the thrust stand. The remaining drift source is generally of smaller magnitude and consists of the thermal drift of the coil shunt resistance compared to the nominal value during calibration, the primary factor of interest is the resistor's temperature sensitivity.

The next two sources listed in Table 1 account for statistical variation of the calibration process. The calibration slope repeatability is a measure of the variability of the calibration procedure. For a simple linear regression calibration method this may be estimated as the standard deviation of the slope of a large number of calibrations. This term may be partially accounted for by other terms, but it is included as a way to capture otherwise difficult day-to-day or user-to-user variability. The term can be expressed as a function of nominal thrust and voltage or as a function of thrust alone, to help aid in understanding. The seventh term, calibration regression correlation, provides a means of quantifying the goodness-of-fit of the calibration regression. A poor calibration dataset will result in a large calibration

regression correlation uncertainty. The relative uncertainty source listed in the table is specifically assuming a linear regression calibration, but other regression correlation estimates could be formulated.

The eight source is the data acquisition (DAQ) uncertainty and accounts for the accuracy and possible thermal drift of the DAQ. The source of uncertainty is introduced anytime that a voltage measurement is made either during calibration or in thrust measurement. As a result, the total uncertainty due to DAQ uncertainty will be the result of combining several similar terms. The term can be expressed as a function of nominal voltage or nominal thrust to aid in understanding.

The last term in Table 1 accounts for the uncertainty of the calibration mechanism (shown in Figure 2b). Additional details of the sources of calibration uncertainty are outlined in Table 2. The calibration alignment source is similar to the thrust vector source of Table 1, and is characterized by the miss-alignment angle of the calibration mechanism. Calibration pulley moment is a term which accounts for the moment introduced by the pulley to effectively remove load from the calibration mechanism. The calibration mass term accounts for the uncertainty in each individual calibration mass. Finally, the gravity uncertainty term accounts for the uncertainty introduced by measuring mass and calculating calibration load from assuming a constant acceleration due to gravity.

Table 2: Sources of calibration uncertainty

Source	Relative Uncertainty	Parameters of Interest	Parameter Description
Calibration alignment	$e_\varphi = 1 - \cos(\varphi)$	φ	Calibration alignment angle
Calibration pulley moment	$e_M = \frac{M}{r\bar{C}_i}$	M	Calibration pulley moment
Calibration mass uncertainty	$e_{m_i} = \frac{U_{m_i} g}{\bar{C}_i}$	U_{m_i}	Calibration mass uncertainty
Calibration gravity uncertainty	$e_g = \frac{U_g}{g}$	U_g	Calibration gravity uncertainty

C. Calculating Uncertainty

For this work, calibrations were regressed using a simple linear regression formula. As a result, the measured thrust and total uncertainty can be expressed as,

$$T = a + b\,V_T \pm U_T,$$

a more detailed expression of the measured thrust can be obtained by evaluating the regression coefficients. Regression coefficients a and b have been calculated from a linear least squares regression of a dataset of n calibration points consisting of C_i and V_i data as,

$$T = \frac{\sum C_i}{n} + \left(V_T - \frac{\sum V_i}{n}\right)\left[\frac{n(\sum V_i C_i) - \sum V_i \sum C_i}{n(\sum V_i^2) - (\sum V_i)^2}\right] \pm U_T.$$

The total relative thrust uncertainty is composed of the nine sources listed in Table 1. The combination of the nine relative uncertainty sources is done using an RSS type methods as,

$$e_T = \frac{U_T}{\bar{T}} = \sqrt{e_\theta^2 + e_x^2 + e_{\dot{x}}^2 + e_\gamma^2 + e_{shunt}^2 + e_{slope}^2 + e_{S_{xy}}^2 + e_{V_i}^2\sqrt{n} + e_{C_i}^2\sqrt{n}}.$$

The DAQ uncertainty e_{V_i} and calibration uncertainty e_{C_i} have been multiplied by a factor of $\sqrt{n}$ to account for the uncertainty introduced by each calibration point. As a result, the terms $e_{V_i}^2\sqrt{n}$ and $e_{C_i}^2\sqrt{n}$ represent the total DAQ and total calibration uncertainty, respectively. As an example, to aid in clarity, the propagation of calibration and DAQ uncertainty are extended in further detail. The propagation of calibration uncertainty to total thrust can be shown to be,

$$e_{C_i} = \frac{1}{\overline{T}}\frac{\partial T}{\partial C_i}U_{C_i} = \frac{U_{C_i}}{\overline{T}}\left\{\frac{1}{n} + \left(\overline{V_T} - \frac{\sum V_j}{n}\right)\left[\frac{nV_i - \sum V_j}{n\left(\sum V_j^2\right) - \left(\sum V_j\right)^2}\right]\right\},$$

where the calibration uncertainty is composed of the four sources listed in Table 2. The four sources of calibration uncertainty were combined again using an RSS type method as,

$$U_{C_i} = \overline{T}\sqrt{e_{\varphi}^2 + e_M^2 + e_{m_i}^2 + e_g^2}.$$

The propagation of DAQ voltage uncertainty is,

$$e_{V_i} = \frac{1}{\overline{T}}\frac{\partial T}{\partial V_i}U_{V_i} = \frac{U_{V_i}}{\overline{T}}\left\{\frac{-1}{n}\left[\frac{n\left(\sum V_j C_j\right) - \sum V_j \sum C_j}{n\left(\sum V_j^2\right) - \left(\sum V_j\right)^2}\right] + \left(\overline{V_T} - \frac{\sum V_j}{n}\right)\frac{\left\{n\left(\sum V_j^2\right) - \left(\sum V_j\right)^2\right\}\{nC_i - \sum C_j\} - \{n\left(\sum V_j C_j\right) - \sum V_j \sum C_j\}\{2nV_i - 2\sum V_j\}}{\left[n\left(\sum V_j^2\right) - \left(\sum V_j\right)^2\right]^2}\right\}.$$

V. Uncertainty Analysis Case Study

As a demonstration of the Uncertainty Quantification method introduced in the previous section, a case study is presented for a specific thrust stand and thruster. The NASA GRC thrust stands in VF-5 and VF-6 have been used to characterize a wide range of electric propulsion thrusters. Specific to this work are the HERMeS TDU thrusters, see references [5-10] for details of the thrusters and testing. The thrust stands in VF-5 and VF-6 are inverted pendulum null-type thrust stands designed for high power Hall thrusters.

The newest implementation is the VF-6 thrust stand, which was slightly modified from the VF-5 baseline. Many of the VF-6 modifications were implemented to assist in quantifying the thrust uncertainty, and improve the reliability of the thrust stand. In general, the uncertainty of the VF-5 and VF-6 thrust stands are believed to be similar. The VF-5 and VF-6 thrust stands use an LVDT position sensor to serve as process variable for the null-coil control circuit. A triangulation laser was implemented in VF-6 to independently observe and record the stand position to high resolution and high sampling rate. The VF-5 and VF-6 thrust stands use an electrolytic inclinometer to serve as process variable for the inclination control circuit. An inertial inclinometer was implemented in VF-6 to independently observe and record the stand inclination to a high resolution. The VF-5 and VF-6 thrust stands have effectively the same in-situ calibration mechanism, consisting of a monofilament with discrete calibration masses and a mechanism for applying the load of the calibration masses to the thrust stand on demand. The thrust stands can be operated in either null-coil mode or displacement mode, during collection of thrust data with TDU null-coil mode was generally used.

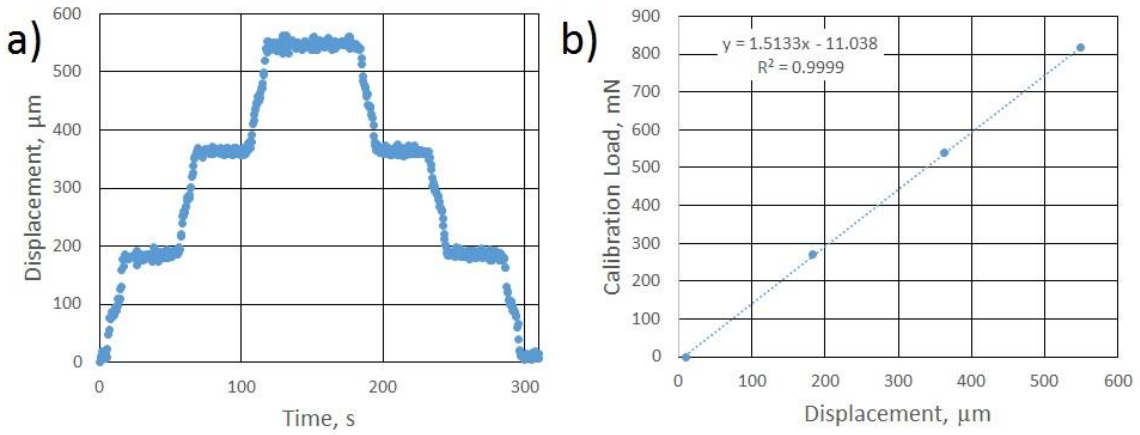

Figure 3. Displacement mode calibration of VF-6. a) Displacement trace during calibration, b) load vs. displacement calibration curve.

To establish the stiffness k the stand is calibrated in displacement mode. Figure 3a shows a typical laser trace during a cycling of the calibration mechanism. Figure 3b is the calibration linear regression between calibration load and displacement, the resulting stand stiffness is 1.51 mN/µm. The stiffness was not used directly for null-coil operation, but was required to establish the uncertainty due to stand displacement drift uncertainty. In null-coil operation the stand is calibrated against the null-coil shunt voltage and the calibration load.

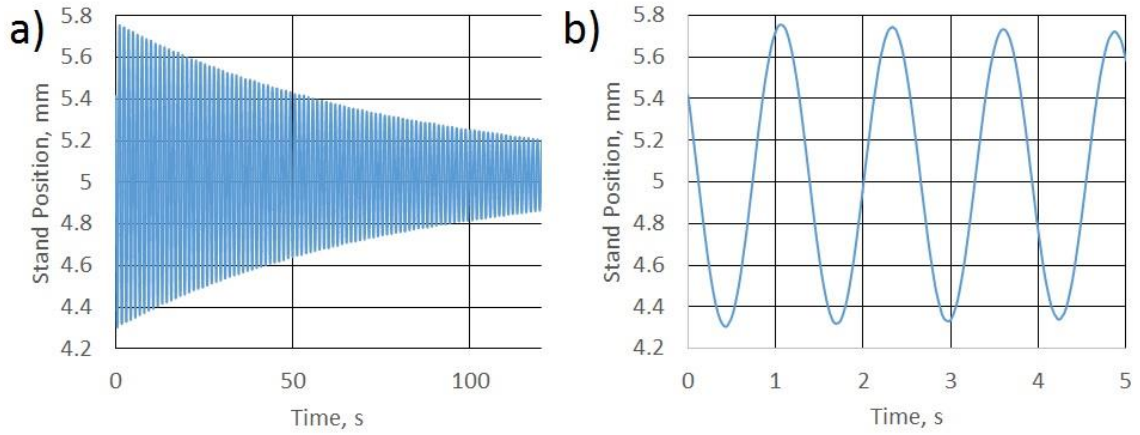

Figure 4. Thrust stand free transient response to medium level external excitation. a) First 120 seconds of natural stand damping and oscillating behavior, b) First 5 seconds to highlight oscillatory behavior.

The free transient response of the thrust stand to excitation is a useful characterization method for the behavior of the stand. Figure 4 shows a 120 second segment of a naturally decaying response to external excitation of the VF-6 thrust stand. The trace in Figure 4 was captured at 2 kHz using a triangulation laser, the laser resolution was <0.5µm. The trace was collected with the TDU thruster mounted on the VF-6 thrust stand while the facility was under vacuum. The trace consists of a periodic oscillation with a decaying amplitude. Guided by the nominal behavior of a simple mass/spring/viscous damper second order system, the free transient response of the system is regressed to the following formula,

$$x(t) = A_1 + A_2 e^{-A_3 t} \sin(A_4 t + A_5),$$

where the A_i coefficients are the unknown regression coefficients [21]. Using the vibrations analysis of a simple mass/spring/viscous damper system, the damping ratio ξ and natural frequency ω_n of the stand can be calculated as,

$$\xi = \frac{1}{\sqrt{\left({}^{A_4}/_{A_3}\right)^2 + 1}},$$
$$\omega_n = \frac{A_3}{\xi}.$$

From damping ratio and natural frequency the stand stiffness k and damping coefficient c can be estimated as,

$$k = m\omega_n^2 = (m_{TDU} + m_{stand})\omega_n^2,$$
$$c = 2\xi m\omega_n = 2\xi(m_{TDU} + m_{stand})\omega_n.$$

With the stand stiffness measured by the displacement mode calibration of Figure 3, an accurate measurement of the total dynamic mass can be made. The total dynamic mass includes both the mass of the TDU thruster and the mass of any moving components of the thrust stand which may include mounting brackets, electrical interface hardware, propellant interface hardware, sensors, and components of the thrust stand itself. The TDU mass m_{TDU} is measured to be 46.7 kg, including the thruster and the thruster mounting bracket. The unknown dynamic mass of the stand can then be determined as,

$$m_{stand} = \frac{k}{\omega_n^2} - m_{TDU}.$$

Determining the stand stiffness, damping coefficient, stand mass, TDU mass, and TDU nominal thrust level are the first step in determining the drift type uncertainty sources of Table 1. The natural frequency, stand mass, and damping coefficient were calculated for three different excitation levels of the thrust stand. Table 3 lists the natural frequency, stand mass, and damping coefficient relative to a low, medium, and high disturbance level. The magnitude of the disturbance level was quantified using the maximum amplitude measured during the trial. The low and medium trials provide relatively consistent results for the parameters. The high disturbance trial exhibited low damping coefficients, accompanied by a non-characteristic transient trace. It is believed that the high disturbance level may be beyond the linear response range of the stand, and should be ignored for nominal operation uncertainty quantification.

The drift terms introduced in Table 1 demonstrate that relative uncertainty is proportional to stand stiffness to thrust ratio $k/\bar{T}$, stand damping coefficient to thrust ratio $c/\bar{T}$, and thruster weight to thrust ratio $mg/\bar{T}$. As a general guideline it is advisable from an uncertainty point of view to minimize these terms. However, additional consideration must be made in the minimization of these terms. For instance, significantly reducing stand stiffness for fixed thruster mass will also reduce the stand natural frequency, which will limit the transient responsiveness of the stand. As a result, the enhanced uncertainty benefit of a lower stand stiffness may hinder the temporal resolution of the thrust data. With TDU operating at 590mN, the stand stiffness to thrust ratio $k/\bar{T}$ is 2.54mm^{-1}, stand damping coefficient to thrust ratio $c/\bar{T}$ is 2.54s/m, and total weight to thrust ratio $mg/\bar{T}$ is 1023mN/mN. As a general guideline VF-5 and VF-6 stiffness was tuned to have a target natural frequency around 1 Hz, as a balance between low uncertainty and reasonable temporal resolution.

Table 3: Thrust stand behavior at three disturbance levels

Disturbance Level	Max. Amplitude (mm)	Natural Freq. (Hz)	Stand Mass (kg)	Damping Coef. (kg/s)
Low	0.06	0.788	14.9	1.55
Medium	0.73	0.788	14.9	1.51
High	1.67	0.787	15.0	0.53

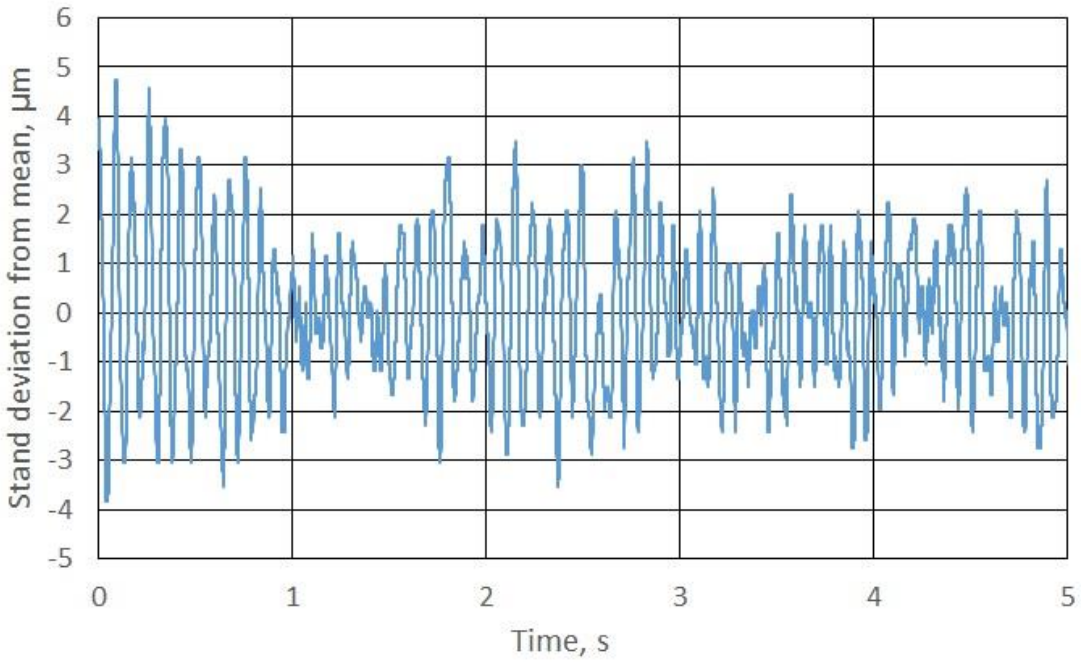

Figure 5. Stand position deviation from mean during nominal operation.

The VF-6 triangulation laser was also used to track the nominal steady behavior of the thrust stand. Figure 5 shows the position trace of the VF-6 thrust stand under vacuum with TDU. The trace was collected after the thrust stand was allowed to stabilize over 24 hours with the thruster in an off state, and the null coil operating nominally. The trace in Figure 5 is a five second snapshot of the nominal behavior of the stand, note that the units on the ordinate axis are in micrometers with the majority of the data collected within ±1µm of the mean. Fast Fourier transform of the trace highlight the dominant unknown 12 Hz noise along with the expected ~1 Hz natural frequency of the thrust stand. No 60 Hz electrical noise or other significant frequencies were observed in the dataset. The 12 Hz noise is likely an artifact of the null-coil control system which uses a low-pass analog filter with a tunable cut-off frequency, or a result of various free components on the stand such as propellant feed lines. Given the small deviation of the thrust stand position during nominal null-coil operation, the 12 Hz noise was not further investigated, but may be considered for future work.

Table 4 provides a summary of the values assumed for VF-6 with TDU targeting a 95% confidence level where appropriate. The stiffness k, damping coefficient c, and weight mg have already been addressed using the displacement mode calibration and triangulation laser traces. The drift state difference terms of Table 1 have been estimated by collecting stand position, velocity, and inclination data from the laser and inertial inclinometer during many calibration cycles. The maximum deviation of the position, velocity, and inclination during a calibration run represents a combination of the control resolution, the steady-state controller error, and any unknown sources. Table 4 lists the maximum state differences for position drift difference $|x_T - \widetilde{x_t}|$, velocity drift difference $|\dot{x}_T - \widetilde{\dot{x}_t}|$, and inclination drift difference $|\gamma_T - \widetilde{\gamma_t}|$. The shunt thermal sensitivity α was pulled from the product literature on the resistor and the estimated temperature difference was conservatively estimated to be 10ºC based on experience and measurement with a thermal infrared camera. The thrust vector mis-alignment angle θ was assumed to be no greater than 2º. A concurrent study at NASA GRC is developing a thrust vector diagnostic system to assist in better approximating this magnitude, see reference [23]. The calibration slope repeatability was calculated as the standard deviation of a set of 47 calibration runs spanning day-to-day operation for two months. The calibration pulley moment M was estimated from a spin down experiment on the pulley. The pulley was spun at a known small angular velocity and was allowed to spin until the retarding moment caused the pulley to come to a stop. Conservation of angular momentum of the pulley was used to estimate the pulley moment. The estimated moment of inertial I_o, initial angular velocity ω, and the measured time to stop t were used to estimate the pulley moment as,

$$M = \frac{I_o \omega}{t}.$$

The calibration alignment angle φ was estimated to be no greater than 2º. The calibration mass uncertainty U_{m_i} was estimated from finding the maximum deviation of repeatedly measuring a set of calibration masses over the course of several months. A significant portion of the uncertainty was found to be due to the inherent stiffness of the monofilament calibration string. Depending on the orientation and bend radius of the monofilament during the mass measurement a range of masses could be recorded. In general, it is advisable to use a configuration which best matches the behavior of the in-situ calibration mechanism. The acceleration due to gravity uncertainty U_g was estimated from the geodetic reference system of 1980 [24]. The assumed acceleration due to gravity of this work was 9.81 m/s^2. The geodetic reference system of 1980 acceleration due to gravity at the latitude of VF-5 and VF-6 (41.4161ºN) is 9.80297 m/s^2. The difference between the two values was rounded up to 0.01 m/s^2 to serve as the U_g uncertainty. The rated 10V range DAQ resolution is 76 µV and the rated DAQ accuracy is 575 µV [25]. Accuracy was calculated based on a worst-case scenario consisting of one year from calibration and operation at 10ºC above the calibration temperature. Based on the rated accuracy the DAQ uncertainty U_{v_i} was estimated to be no greater than 600 µV. Table 5 includes an example null-coil calibration data set which was used for estimating the calibration regression correlation uncertainty, regression coefficients, and nominal voltage.

Table 4: Values assumed for analysis of VF-5/VF-6 thrust stand with TDU

Parameter	Term	Assumed Value
TDU Mass	m_{TDU}	46.7 kg
Stand Mass	m_{Stand}	14.9 kg
Total Weight	mg	604 N
Stand natural frequency	ω_n	0.788 Hz
Stand damping coefficient	c	1.5 kg/s
Stand position drift	$\lvert x_T - \widetilde{x_t}\rvert$	2.4µm
Stand velocity drift	$\lvert \dot{x}_T - \widetilde{\dot{x}_t}\rvert$	0.3 mm/s
Stand inclination drift	$\lvert \gamma_T - \widetilde{\gamma_t}\rvert$	2.0 arc seconds
Shunt thermal sensitivity	α	100 ppm/ºC
Shunt thermal drift	$\lvert t_T - \widetilde{t_t}\rvert$	10ºC
Thrust vector alignment angle	θ	2.0º
Calibration slope repeatability	S_b	1.54 mN/V
DAQ uncertainty	U_{v_i}	600 µV
Calibration pulley moment	M	2.7e-6 Nm
Calibration alignment angle	φ	2.0º
Calibration mass uncertainty	U_{m_i}	0.1 g
Gravity uncertainty	U_g	0.01 m/s^2

Table 5: Example null-coil calibration dataset

Calibration Load (mN)	Null coil shunt (mV)
0	19.2
277.9	-171
549.2	-356
823.3	-543
823.3	-544
549.2	-357
277.9	-171
0	19.3

Applying the values in Tables 4 and 5 to the Uncertainty Quantification method introduced in the previous section results in Table 6, Table 7, Figure 6, and Figure 7. Table 6 summarizes the distribution of the eight uncertainty sources outlined in Table 1. Table 6 also includes an estimation of the total thrust uncertainty as a relative error percent. The uncertainty distributions were generated for two nominal thrust levels to highlight the influence of thrust level on the different sources. The 600mN thrust level is representative of the nominal operating point for TDU and should be regarded as the main values. The 100mN thrust levels are generated only to highlight the influence of thrust level. Thrust vector is independent of thrust as it only depends on the angle assumed, otherwise the sources were inversely

proportional to thrust. The two dominant sources of uncertainty were stand inclination drift and stand displacement drift, which highlights the importance of designing thrust stands to carefully monitor inclination and position drift. The next largest sources of uncertainty were stand velocity drift, DAQ uncertainty, and calibration uncertainty. The Pareto plots of Figure 6 highlight the contribution of the significant sources. The smallest sources were calibration slope repeatability, thrust vector, shunt thermal drift, and linear regression correlation. The individual components of calibration uncertainty are summarized in Table 7. The calibration sources of uncertainty are independent of thruster operation, so the values are identical for a calculation at any thrust level. The largest source of calibration uncertainty was alignment followed by mass uncertainty, gravity uncertainty, and pulley moment.

Table 6: Uncertainty source distribution

Relative Uncertainty Source	Percent at 100mN Nominal	Percent at 600mN Nominal
Thrust vector	6.1e-2	6.1e-2
Stand displacement drift	3.6e0	6.0e-1
Stand velocity drift	4.5e-1	7.5e-2
Stand inclination drift	5.8e0	9.7e-1
Shunt thermal drift	5.0e-2	5.0e-2
Calibration slope repeatability	7.6e-2	1.0e-1
Calibration linear regression correlation	4.0e-4	1.0e-4
Total DAQ uncertainty	4.5e-1	9.4e-2
Total calibration uncertainty	5.3e-1	1.5e-1
TOTAL	**6.9**	**1.1**

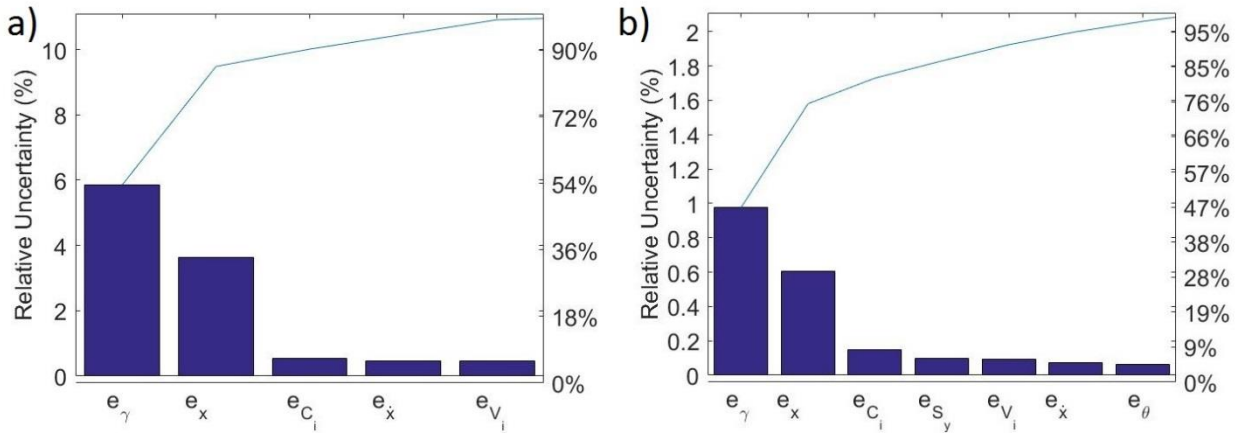

Figure 6. Pareto plots of the leading sources of uncertainty for a) 100mN operating point and b) 600mN operating point.

Table 7: Calibration uncertainty source distribution

Relative Uncertainty Source	Percent
Calibration alignment	6.1e-1
Calibration pulley moment	3.1e-2
Calibration mass uncertainty	3.5e-1
Calibration gravity uncertainty	1.0e-1

The variation in thrust uncertainty is shown in Figure 7 for VF-6 and VF-5 stands with TDU. The nominal thrust levels range from 100mN to 600mN for demonstration purposes. A more realistic thrust range for TDU operation is 400 to 600mN. Over the full 100 to 600mN range the total relative thrust uncertainty spans 6.9 to 1.1%. Over the same range the absolute thrust uncertainty spans 6.92 to 6.97 mN. The significant increase in relative uncertainty at low thrust levels highlights the importance of tuning a thrust stand to operate for a given thruster, rather than relying on a single configuration for all thrusters. The most critical parameters to consider tuning are the stand stiffness, stand mass, thruster mass, calibration masses, null-coil settings, and the DAQ configuration.

A thrust stand monitoring strategy can be used to ensure the reliability of thrust stand data. Since the two largest sources of uncertainty are stand displacement drift and stand inclination drift a system can be setup to continuously monitor changes in displacement and inclination. If an acceptable level of uncertainty can be determined, the stand stiffness to thrust ratio $k/\bar{T}$, and thruster weight to thrust ratio $mg/\bar{T}$ are all known, then a limit for the maximum position drift difference $|x_T - \tilde{x}_i|$ and inclination drift difference $|\gamma_T - \tilde{\gamma}_i|$ can be established. With established limits of acceptable drift a latching monitoring system can ensure that thrust data is reliable to within acceptable levels of thrust uncertainty.

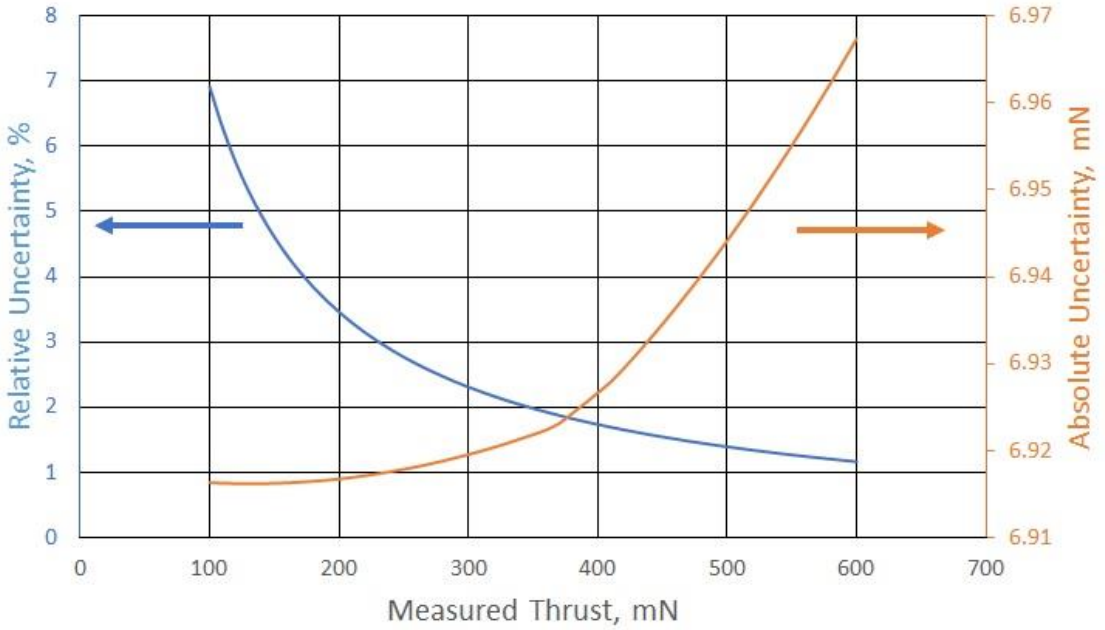

Figure 7. Total uncertainty of TDU in VF-5 and VF-6 thrust stands.

VI. Future Work

Future work may include evaluating different thrusters and different thrust stands, with focus on covering a wider span of thrust levels. Some limited uncertainty analysis of various thrusters on the VF-5 and VF-6 thrust stands has been underway, but is not yet complete to the level of the TDU work. Additional future work may extend to consider other thrust stand configurations including torsional thrust stands. NASA GRC is currently working on fabricating a new inverted pendulum thrust stand for Vacuum Facility 11 (VF-11). The VF-11 thrust stand will be similar to VF-6 in that it will be incorporated with multiple sensors to best establish uncertainty values. The VF-11 thrust stand will help provide a smaller scale thrust stand for detailed uncertainty work. Finally, the uncertainty analysis is an ever changing model which grows with every experiment. As new uncertainty sources are identified and quantified, or existing sources are better quantified the analysis can improve.

VII. Conclusion

The uncertainty of an inverted pendulum null-coil thrust stand has been quantified. Several sources of uncertainty have been considered and estimates of magnitude have been calculated. The propagation of uncertainty to thrust has been outlined and demonstrated with a case study on NASA Glenn Research Center's Vacuum Facility 6. A summary of all assumptions has been provided along with the necessary formulas to implement the calculation. A summary of relative and absolute uncertainty has been presented and the magnitude of different sources has been discussed. It has been determined that the leading sources of uncertainty are thrust stand displacement drift and inclination drift. A strategy for monitoring the position and inclination has been recommended to provide high quality thrust data. Suggestions for ensuring a well matched thrust stand and thruster combination will also ensure minimization of the largest sources of uncertainty. Design of future stands and operation of existing stands should consider the sources of uncertainty addressed by this work. Whenever possible the analysis has been generalized to be extended to other thrust stands and thrusters. For the case study of this work the thrust was found to be ±6.9mN over a wide range of thrust levels.

Acknowledgments

The authors would like to thank the Space Technology Mission Directorate in support of the Solar Electric Propulsion Technology Demonstration Mission Project for funding the joint NASA GRC and JPL development of the Advanced Electric Propulsion System. The authors would like to give a special thanks to John Yim for his insightful reviews of the work.

References

[1] Congress, "National Aeronautics and Space Administration Transition Authorization Act of 2017," ed, 2017.

[2] W. Gerstenmaier, "Progress in Defining the Deep Space Gateway and Transport Plan," in *NASA Advisory Council Human Exploration and Operations Committee Meeting*, Washington, DC, 2017.

[3] B. K. Smith, M. L. Nazario, and C. C. Cunningham, "Solar Electric Propulsion Vehicle Demonstration to Support Future Space Exploration Missions," in *Space Propulsion 2012*, Bordeaux, France, 2012.

[4] M. J. Patterson and J. S. Sovey, "History of Electric Propulsion at NASA Glenn Research Center: 1956 to Present," *Journal of Aerospace Engineering*, vol. 26, pp. 300-316, 2013.

[5] H. Kamhawi, W. Huang, T. Haag, R. Shastry, R. E. Thomas, J. T. Yim, D. A. Herman, G. Williams, J. Myers, R. R. Hofer, I. Mikellides, M. J. Sekerak, and J. E. Polk, "Performance and Facility Background Pressure Characterization Tests of NASA's 12.5-kW Hall Effect Rocket with Magnetic Shielding Thruster," presented at the 34th International Electric Propulsion Conference, Kobe, Japan, 2015.

[6] H. Kamhawi, T. W. Haag, W. Huang, D. A. Herman, G. J. Williams, P. Y. Peterson, R. R. Hofer, and I. Mikellides, "Performance, Stability, and Pressure Effects Characterization Tests of NASA's 12.5-kW Hall Effect Rocket with Magnetic Shielding (HERMeS) Thruster," in *52nd AIAA/SAE/ASEE Joint Propulsion Conference*, Salt Lake City, UT, 2016.

[7] P. Y. Peterson, H. Kamhawi, W. Huang, G. Williams, J. Gilland, J. Yim, R. R. Hofer, and D. Herman, "NASA's HERMeS Hall Thruster Electrical Configuration Characterization," presented at the 52nd AIAA/ASME/SAE/ASEE Joint Propulsion Conference, AIAA-2016-5027, Salt Lake City, UT, 2016.

[8] H. Kamhawi, W. Huang, J. H. Gilland, T. Haag, J. Mackey, J. Yim, L. Pinero, G. Williams, P. Y. Peterson, and D. Herman, "Performance, Stability, and Plume Characterization of the HERMeS Thruster with Boron Nitride Silica Composite Discharge Channel," presented at the 35th International Electric Propulsion Conference, IEPC-2017-392, Atlanta, GA, 2017.

[9] P. Y. Peterson, H. Kamhawi, W. Huang, J. Yim, T. W. Haag, J. Mackey, M. McVetta, L. Sorrelle, T. Tomsik, R. Gilligand, and D. Herman, "Reconfiguration of NASA GRC's Vacuum Facility 6 for Testing of Advanced Electric Propulsion System (AEPS) Hardware," presented at the 35th International Electric Propulsion Conference, IEPC-2017-028, Atlanta, GA, 2017.

[10] P. Y. Peterson, J. D. Frieman, H. Kamhawi, G. Williams, J. H. Gilland, R. Hofer, and D. Herman, "NASA HERMeS Hall Thruster Long Duration Wear Test," in *65th JANNAF Propulsion Meeting*, Long Beach, CA, 2018.

[11] T. W. Haag, "Thrust Stand for High-Power Electric Propulsion Devices," *Review of Scientific Instruments*, vol. 62, pp. 1186-1191, May 1991 1991.

[12] T. W. Haag, "Thrust stand for pulsed plasma thrusters," *Review of Scientific Instruments*, vol. 68, pp. 2060-2067, 1997.

[13] J. E. Polk, A. Pancotti, T. Haag, S. King, M. Walker, J. Blakely, and J. Ziemer, "Recommended Practice for Thrust Measurement in Electric Propulsion Testing," *Journal of Propulsion and Power*, vol. 33, pp. 539-555, 2017.

[14] T. W. Haag, "Thrust stand for high-power electric propulsion devices," *Review of Scientific Instruments*, vol. 62, pp. 1186-1191, 1991.

[15] K. G. Xu and M. L. R. Walker, "High-power, null-type, inverted pendulum thrust stand," *Review of Scientific Instruments*, vol. 80, 2009 2009.

[16] K. D. Diamant, J. E. Pollard, M. W. Crofton, M. J. Patterson, and G. C. Soulas, "Thrust Stand Characterization of the NASA Evolutionary Xenon Thruster," *Journal of Propulsion and Power*, vol. 27, pp. 777-785, 2011.

[17] S. J. Hall, A. D. Gallimore, and E. Viges, "Thrust Stand for Very-high-power Hall Thrusters," *JANNAF 8th Spacecraft Propulsion Subcomitee Meeting*, 2016-0006CX, 2016.

[18] R. S. Figliola and D. E. Beasley, "Theory and Design for Mechanical Measurements 3rd," Wiley, 2014.

[19] R. B. Abernethy, R. P. Benedict, and R. B. Dowdell, "ASME Measurement Uncertainty," *Journal of Fluids Engineering*, Vol. 107, 1985.

[20] R. J. Moffat, "Contributions to the Theory of Single-Sample Uncertainty Analysis," *Transaction of the ASME*, Vol. 104, 1982.
[21] S. Castrup, H. T. Castrup, et. al, "Measurement Uncertainty Analysis Principles and Methods," National Aeronautics and Space Administration, NASA-HDBK-8739.19-3, 2010.
[22] J. G. Kelly, "Mechancial Vibrations: Theory and Applications, SI," *Cengage Learning*, ISBN-10: 1-4390-6214-5 (2012).
[23] G. F. Benavides, J. A. Mackey, R. E. Thomas, and D. M. Ahern, "Diagnostic for Verifying the Thrust Vector Requirement of the AEPS Hall-Effect Thruster and Comparison to the NEXT-C Thrust Vector Diagnostic," Joint Propulsion Conference, 2018 (In press).
[24] H. Moritz, " Geodetic reference system 1980," *Bulletin géodésique*, *58*(3), pp. 388-398, 1984.
[25] Keysight Technologies 34980A Multifunction Switch/Measure Unit, www.keysight.com, August 3 2014.